

## PAPER

[View Article Online](#)  
[View Journal](#) | [View Issue](#)Cite this: *Dalton Trans.*, 2025, **54**, 9418

## Enhancing electrocatalytic water oxidation: ligand complementarity in ternary Cu(II) complexes†

Pranjal Das,<sup>a,b</sup> Hemrupa Kuilya,<sup>a</sup> Swati Basak,<sup>a,b</sup> Baisali Hazarika,<sup>a,b</sup> Joydeep Ray,<sup>c</sup> Debajit Sarma,<sup>b</sup> Diganta Choudhury<sup>a</sup> and Apurba Kalita<sup>ID</sup> \*<sup>a</sup>

The electrocatalytic water oxidation activity of two mononuclear ternary copper(II) complexes, **1**, [Cu(bipy)(HL<sub>1</sub>)](ClO<sub>4</sub>)<sub>2</sub>, [bipy = 2,2'-bipyridine, HL<sub>1</sub> = N<sup>1</sup>-(2-aminoethyl)ethane-1,2-diamine] and **2**, [Cu(phen)(HL<sub>1</sub>)](ClO<sub>4</sub>)<sub>2</sub>, [phen = 1,10-phenanthroline], has been investigated. Complexes **1** and **2** exhibit turnover frequencies (TOF) of 483 s<sup>-1</sup> and 445 s<sup>-1</sup> at overpotentials of approximately 453 mV and 493 mV, respectively, in neutral phosphate buffer. These ternary complexes demonstrate superior catalytic performance compared to their binary counterparts. In these ternary complexes, both ligands act complementarily to enhance stability and redox activity, which are crucial for catalytic performance of the metal complexes. Electrochemical investigations further reveal that the structural flexibility of the aliphatic amine ligand moiety influences the overall catalytic efficiency of the ternary metal complexes.

Received 2nd April 2025,  
Accepted 14th May 2025

DOI: 10.1039/d5dt00790a

rsc.li/dalton

## Introduction

The escalating global energy demand, driven by population growth, industrialization, and economic development, poses a critical challenge for energy sustainability. As the global community grapples with the climate crisis caused by the overuse of traditional fossil fuel reserves, the pursuit of sustainable and eco-friendly renewable energy sources has become imperative. In this regard, green hydrogen produced by the electrolysis of water emerges as a potential alternative fuel.<sup>1–3</sup> The efficiency of the production of green hydrogen from water is directly proportional to the rate of the water oxidation reaction, a critical step involving transfer of four electrons and four protons to form the O–O bond. In nature, this reaction is efficiently catalysed by the CaMn<sub>4</sub>O<sub>5</sub> cluster within the oxygen-evolving complex (OEC) of photosystem II (PSII).<sup>4</sup> Researchers have attempted to replicate the efficiency of OEC using various transition metal complexes.<sup>5–33</sup>

Among the various alternatives for electrocatalytic water oxidation catalysts, copper (Cu) complexes have gained significant attention due to their abundance, cost effectiveness, and tuneable catalytic properties.<sup>10–33</sup> Since the first report of a copper-bipyridine water-oxidation electrocatalyst by Mayer and co-

workers in 2012, there has been a rapid expansion in the study of copper complexes.<sup>10</sup> A significant number of complexes with bipyridine-based ligand environments have been reported to exhibit electrocatalytic water oxidation activity.<sup>10,23,29–32</sup> However, achieving catalytic performance suitable for practical applications remains a challenge. Notably, the inner coordination sphere of metal complexes plays a crucial role in determining their overall catalytic efficiency.

The structural rigidity and flexibility of the ligand framework have also been reported to influence the catalytic activity of metal complexes.<sup>21–26</sup> A rigid ligand can make a complex inert, enhancing its stability under harsh catalytic conditions, whereas a flexible ligand may allow the metal complex to undergo necessary structural changes during the catalytic cycle. In this regard, ternary metal complexes that incorporate structurally diverse ligand frameworks offer the possibility of fine-tuning the structural effects of the ligands to achieve optimal catalytic activity.

In this study, we report the catalytic activity of two mononuclear ternary copper(II) complexes, **1**, [Cu(bipy)(HL<sub>1</sub>)](ClO<sub>4</sub>)<sub>2</sub>, [bipy = 2,2'-bipyridine, HL<sub>1</sub> = N<sup>1</sup>-(2-aminoethyl)ethane-1,2-diamine] and **2**, [Cu(phen)(HL<sub>1</sub>)](ClO<sub>4</sub>)<sub>2</sub>, [phen = 1,10-phenanthroline]. Ternary complexes **1** and **2** exhibit superior catalytic activity in neutral phosphate buffer compared to their binary counterparts.

## Results and discussion

## Synthesis and characterization

Ternary copper(II) complexes, **1** and **2**, were synthesized using the bidentate ligands bipyridine (bipy) and phenanthroline

<sup>a</sup>Department of Chemistry, B. Borooah College, Guwahati 781007, Assam, India.  
E-mail: apurbakalitabbc@gmail.com

<sup>b</sup>Department of Chemistry, Gauhati University, Guwahati 781014, Assam, India

<sup>c</sup>Department of Chemistry, IIT Patna, Patna 801103, Bihar, India

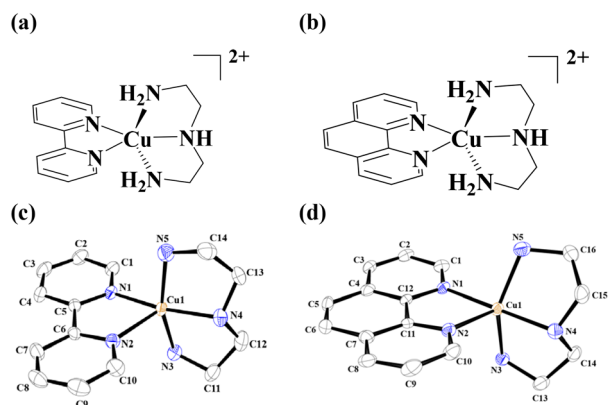
†Electronic supplementary information (ESI) available: Experimental procedures, FT-IR, UV-visible, and crystallographic data. CCDC 2401171, 2401172, 2435313–2435318. For ESI and crystallographic data in CIF or other electronic format see DOI: <https://doi.org/10.1039/d5dt00790a>

(phen), respectively, along with the tridentate ligand **HL**<sub>1</sub>, as their perchlorate salts (see the Experimental section for details). Complexes were characterized by different spectroscopic as well as by powder and single crystal X-ray diffraction techniques. The single-crystal X-ray structure of the complexes (Fig. 1) revealed that in both complexes copper is coordinated to five nitrogen donor atoms. Crystallographic data are given in Table S1.† The powder XRD pattern of the bulk sample of the complexes closely resembles the simulated pattern (Fig. S10†). The UV-visible spectra of complexes **1** and **2**, in a neutral phosphate buffer, exhibit a broad d-d band at  $\lambda_{\text{max}}$  ( $\epsilon/\text{M}^{-1}\text{cm}^{-1}$ ): 651 nm (175) and 632 nm (171), along with relatively strong intra-ligand absorptions in the UV region (Fig. S13†). The UV-visible spectra of the complexes recorded in water and buffer medium are found to be identical (Fig. S14 and S15†). The phosphate buffer solution of the complexes was found to display a characteristic four line EPR spectrum at room temperature (Fig. S25†).

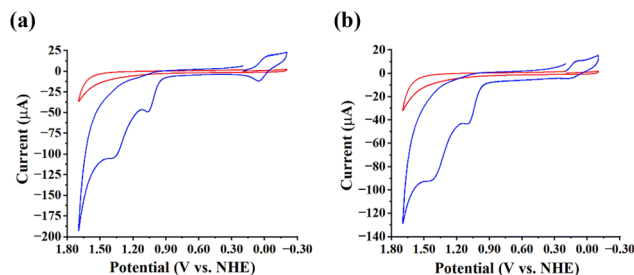
### Redox properties

To explore the electrocatalytic activity of the copper complexes, cyclic voltammograms (CVs) and differential pulse voltammograms (DPVs) were recorded in 0.1 M neutral sodium phosphate buffer using glassy carbon (GC) as the working electrode, Ag/AgCl as the reference electrode and a platinum wire as the counter electrode in a single compartment electrochemical cell. Potentials are reported *versus* the normal hydrogen electrode (NHE) through the addition of 0.197 V to the measured potential.

The cyclic voltammograms (CVs) of 1 mM solutions of complexes **1** and **2** are shown in Fig. 2. The onset potentials for water oxidation are located near 1.27 V and 1.31 V *vs.* NHE for complexes **1** and **2**, respectively. These values were determined from the half-peak potential of the catalytic wave observed in the CVs of the complexes (Fig. S26†).<sup>13</sup> For complexes **1** and **2**, the overpotentials at which water oxidation occurs were determined to be 453 mV and 493 mV, respectively.



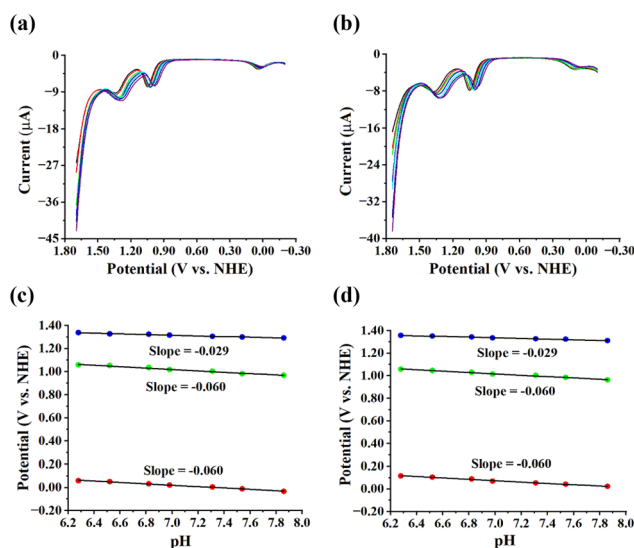
**Fig. 1** Structures of (a) complex **1** and (b) complex **2**. ORTEP diagram of (c) complex **1** and (d) complex **2** (50% thermal ellipsoid plot). In the ORTEP diagram, hydrogen atoms and perchlorate ions are not shown for clarity.



**Fig. 2** Cyclic voltammograms of 1 mM solution of (a) complex **1** (blue line) and (b) complex **2** (blue line) in 0.1 M neutral phosphate buffer at a scan rate of  $100\text{ mV s}^{-1}$ . The red line indicates the cyclic voltammogram of 0.1 M neutral phosphate buffer in the absence of the catalyst at a scan rate of  $100\text{ mV s}^{-1}$ .

The differential pulse voltammograms (DPVs) (Fig. 3) of complexes **1** and **2** in neutral phosphate buffer exhibited three anodic peaks in a potential range from  $-0.30\text{ V}$  to  $+1.70\text{ V vs. NHE}$ . The first anodic peaks for complexes **1** and **2** in neutral phosphate buffer appear at around  $0.02\text{ V}$  and  $0.07\text{ V vs. NHE}$ , respectively. This electrochemically quasi-reversible peak shows a pH-dependency of nearly  $0.060\text{ V}$  per pH unit and is assigned to the  $\text{Cu}^{\text{II}}/\text{Cu}^{\text{I}}$  couple.

The second anodic peak appears at  $+1.02\text{ V}$  and  $+1.01\text{ V vs. NHE}$  for complexes **1** and **2** respectively in neutral phosphate buffer. Calculations using Laviron equations<sup>34</sup> (Fig. S27 and S28†) and analysis of the Pourbaix diagrams (Fig. 3) indicate the involvement of two electrons and two protons in this step.



**Fig. 3** Differential pulse voltammograms (DPVs) of (a) complex **1** and (b) complex **2** in 0.1 M phosphate buffer at pH 6.28 (black), 6.52 (red), 6.82 (green), 6.98 (blue), 7.31 (cyan), 7.54 (navy) and 7.86 (purple) conducted under a nitrogen atmosphere at room temperature. Pourbaix diagram of (c) complex **1** and (d) complex **2** depicting the change of potential of the first (red dot), second (green dot) and third (blue dot) anodic peaks with variation of pH of the 0.1 M phosphate buffer medium.

Spectroelectrochemical investigation and comparison of CVs and DPVs obtained from analogous Zn complexes (Fig. S29 and S30†) suggest the formation of a Cu(III) species and concomitant oxidation of the aliphatic ligand moiety at this potential (Scheme 1, Step 1). The DPV of ligand **HL**<sub>1</sub>, *N*<sup>1</sup>-(2-aminoethyl)ethane-1,2-diamine, shows a peak at 1.03 V vs. NHE in neutral phosphate buffer. However, this type of peak was not observed in the DPV of its *N*<sup>1</sup>-methylated form, *N*<sup>1</sup>-(2-aminoethyl)-*N*<sup>1</sup>-methylethane-1,2-diamine (Fig. S31†). This observation suggests that the redox activity of **HL**<sub>1</sub> originates from the oxidation of a secondary amine site of the ligand in the potential range of the second anodic peak of the complexes. Monitoring of the UV-visible spectra of the complexes during controlled potential electrolysis (CPE) at the potential of the second anodic peak shows the formation of a new peak at  $\lambda_{\text{max}}$  ( $\epsilon/\text{M}^{-1}\text{cm}^{-1}$ ): 526 nm (340) and 502 nm (288) for complexes **1** and **2**, respectively, (Fig. S32†). This change in the UV-visible spectra is believed to originate from the formation of a d<sup>8</sup> Cu(III) species, [Cu<sup>III</sup>(bipy)(L<sub>1</sub>')(OH)]<sup>2+</sup> and [Cu<sup>III</sup>(phen)(L<sub>1</sub>')(OH)]<sup>2+</sup>, respectively, for complexes **1** and **2** (Scheme 1, Step 1). A similar assignment of the oxidation potential to the formation of Cu(III) species has been reported in recent studies on copper-based electrocatalysts for the water oxidation reaction.<sup>13,15</sup>

The high oxidizing power that accumulates at this point on the metal complexes drives the reaction with solvent water molecules to form a Cu(II)-hydroperoxo intermediate (Scheme 1, Step 2). The formation of a Cu(II)-hydroperoxo

intermediate during the reaction between Cu(III) reactive species and water molecules is well documented in the literature.<sup>14,18,25,28</sup> The formed Cu(II)-hydroperoxo species further oxidizes at the potential of the third anodic peak to release the oxygen molecule and regenerate the catalyst (Scheme 1, Step 3). Calculations using Laviron equations (Fig. S27 and S28†) and analysis of the Pourbaix diagrams (Fig. 3) indicate the involvement of two electrons and one proton in this step.

### Kinetics of electrocatalysis

The cyclic voltammograms recorded for complexes **1** and **2** at different concentrations revealed that the catalytic current increases linearly with the concentration of the catalyst at a scan rate of 100 mV s<sup>-1</sup> (Fig. S33 and S34†). This first order kinetics suggests a single site mechanism for water oxidation catalysis for both complexes. The dependence of the catalytic current (*i*<sub>cat</sub>) on the catalyst concentration can be described by eqn (1):<sup>35</sup>

$$i_{\text{cat}} = n_{\text{cat}}FA[C](k_{\text{cat}}D_{\text{Cu}})^{1/2} \quad (1)$$

In eqn (1),  $n_{\text{cat}}$  (= 4) is the number of electrons involved in water oxidation, *F* is the Faraday constant, *A* is the area of the working electrode (0.07 cm<sup>2</sup>), [*C*] is the concentration of the catalyst, *k*<sub>cat</sub> is the rate constant for water oxidation and *D*<sub>Cu</sub> is the diffusion coefficient. The value of *D*<sub>Cu</sub> was determined from the plot of anodic peak currents (*i*<sub>d</sub>) of the Cu<sup>II</sup>/Cu<sup>I</sup> couple vs. square root of the scan rates ( $\nu^{1/2}$ ) by using the Randles-Sevcik equation<sup>35</sup> (eqn (2)). The peak current varies linearly with the scan rate for both the complexes and diffusion coefficients of  $12.96 \times 10^{-7} \text{ cm}^2 \text{ s}^{-1}$  and  $11.72 \times 10^{-7} \text{ cm}^2 \text{ s}^{-1}$  were determined for complexes **1** and **2**, respectively (Fig. S35 and S36†).

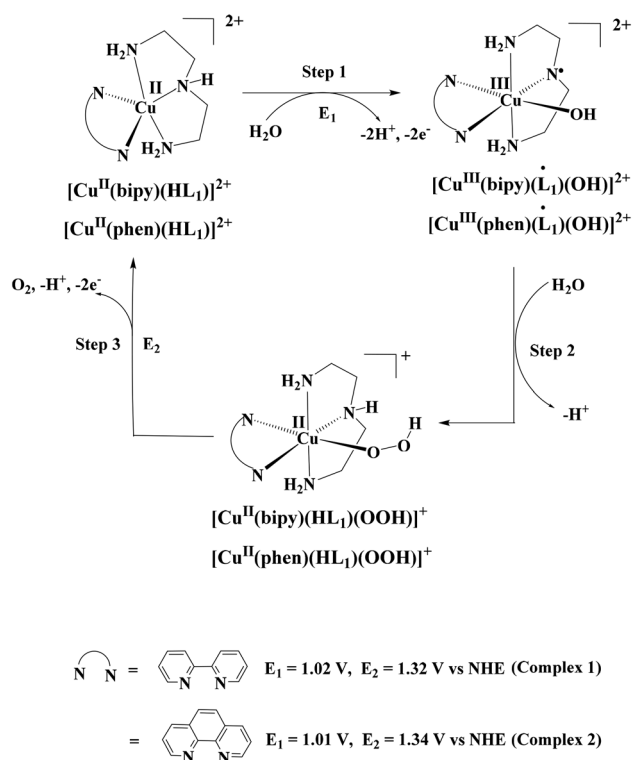
$$i_d = 0.446nFA[C]\{(nF\nu D_{\text{Cu}})/RT\}^{1/2} \quad (2)$$

In eqn (2),  $n$  (= 1e<sup>-</sup>) is the number of electrons involved with the Cu<sup>II</sup>/Cu<sup>I</sup> couple,  $\nu$  is the scan rate, *R* is the ideal gas constant and *T* is the temperature.

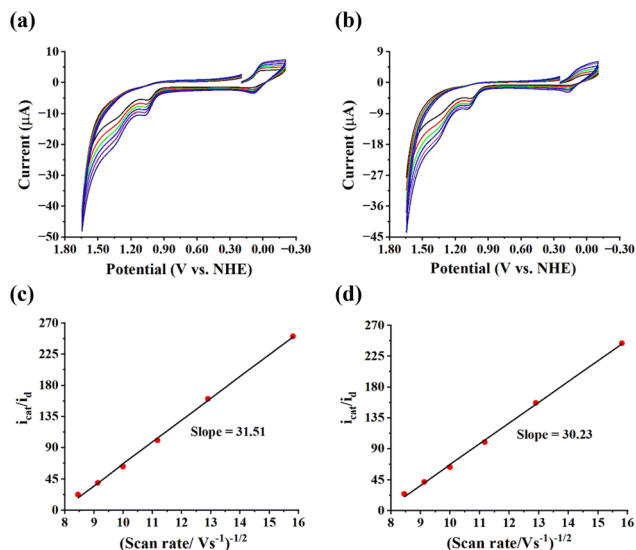
To obtain the kinetic information about the catalytic process, cyclic voltammograms at different scan rates (4–14 mV s<sup>-1</sup>) [Fig. 4(a) and (b)] were recorded for complexes **1** and **2** in 0.1 M neutral phosphate buffer. The value of the catalytic rate constant (*k*<sub>cat</sub>) was determined using eqn (3):<sup>10,22,27</sup>

$$i_{\text{cat}}/i_d = 2.242 (n_{\text{cat}}/n)(RT/nF)^{1/2} (k_{\text{cat}})^{1/2} \nu^{-1/2} \quad (3)$$

In eqn (3), *i*<sub>cat</sub> is the catalytic peak current, *i*<sub>d</sub> is the peak current of the diffusion controlled peak (here we approximate this current to the current associated with the Cu<sup>II</sup>/Cu<sup>I</sup> couple),  $n_{\text{cat}}$  (= 4) is the number of electrons involved in water oxidation,  $n$  (= 1) is the number of electrons involved in non-catalytic peak (here the Cu<sup>II</sup>/Cu<sup>I</sup> couple), *k*<sub>cat</sub> is the catalytic rate constant and  $\nu$  is the scan rate. Now, from the slope of a linear fit line in the plot of  $i_{\text{cat}}/i_d$  against  $\nu^{-1/2}$  [Fig. 4(c) and (d)], the values of *k*<sub>cat</sub> are calculated to be 483 s<sup>-1</sup> and 445 s<sup>-1</sup> for complexes **1** and **2**, respectively. To investigate the impact of



Scheme 1 Proposed catalytic cycle of complexes **1** and **2**.



**Fig. 4** Cyclic voltammograms of (a) complex **1** and (b) complex **2** at 4 (black), 6 (red), 8 (green), 10 (blue), 12 (purple) and 14 (royal) mV s<sup>−1</sup> scan rates in 0.1 M neutral phosphate buffer. Plot of  $i_{\text{cat}}/i_d$  vs.  $\nu^{-1/2}$  for (c) complex **1** and (d) complex **2**.

the buffer base, we have recorded the cyclic voltammograms of complexes **1** and **2** in different concentrations of phosphate buffers (Fig. S37 and S38†). The catalytic current is found to be insensitive to the concentration of phosphate buffer used. This observation implies that phosphate ions do not interfere with the catalytic activity of the complexes.

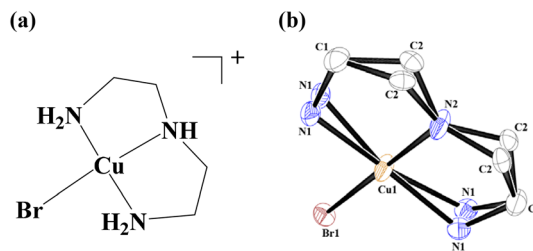
A comparison of scan-rate-normalized CVs ( $i_{\text{cat}}/\nu^{1/2}$ ) at different scan rates shows a decrease in  $i_{\text{cat}}$  with increasing  $\nu$  (Fig. S39†), which is consistent with a contribution to the current from a rate-limiting water oxidation catalysis.<sup>35</sup> CV carried out in D<sub>2</sub>O shows a much smaller catalytic current (Fig. S40†), suggesting that the transfer of proton(s) from H<sub>2</sub>O is a significant component of the rate-determining step. Solvent kinetic isotope effects (KIE) of 2.31 and 2.07 were determined for complexes **1** and **2**, respectively, according to eqn (4):<sup>36,37</sup>

$$\text{KIE} = k_{\text{cat}}(\text{H}_2\text{O})/k_{\text{cat}}(\text{D}_2\text{O}) = [i_{\text{cat}}(\text{H}_2\text{O})/i_{\text{cat}}(\text{D}_2\text{O})]^2 \quad (4)$$

In eqn (4),  $k_{\text{cat}}(\text{H}_2\text{O})$  and  $k_{\text{cat}}(\text{D}_2\text{O})$  are the catalytic rate constants and  $i_{\text{cat}}(\text{H}_2\text{O})$ ,  $i_{\text{cat}}(\text{D}_2\text{O})$  are the catalytic peak currents of complexes measured in H<sub>2</sub>O and D<sub>2</sub>O medium, respectively.

To compare the catalytic activity of ternary complexes with their binary counterparts we have prepared the binary Cu(II) complex, **3**, with ligand **HL**<sub>1</sub> (see the Experimental section). The complex was characterized by various analytical techniques (Experimental section). The single crystal structure of the complex was determined. The perspective ORTEP view of complex **3** is shown in Fig. 5. The crystallographic data are given in Table S2.†

Electrochemical investigation of complex **3** (Fig. S41–S43†) shows that it is catalytically unstable in neutral phosphate buffer and decomposes at the electrode surface during controlled potential electrolysis (CPE). This is evident from the CVs recorded before and after the electrolysis experiment



**Fig. 5** (a) Structure of complex **3** and (b) ORTEP diagram of complex **3** (50% thermal ellipsoid plot); the N1 and C2 atoms are modelled as disordered. In the ORTEP diagram counter ions and hydrogen atoms are not shown for clarity.

(Fig. S42†) and from the SEM and EDX data of the ITO working electrodes used in the CPE experiment (Fig. S43†). We have also prepared the binary copper(II) complexes of bipyridine and phenanthroline (see the ESI†) to compare their catalytic activity with those of complexes **1** and **2**. However, these binary copper(II) complexes of bipyridine and phenanthroline are found to be catalytically inactive in neutral phosphate buffer as evidenced from their cyclic voltammograms recorded in the potential range −0.3 to +1.90 V vs. NHE (Fig. S44 and S45†). The catalytic parameters of some recently reported bipyridine and phenanthroline based copper(II) complexes in an alkaline buffer medium are listed in Table 1.

In comparison with other reported pyridine-based binary complexes, the  $k_{\text{cat}}$  value for ternary complexes **1** and **2** shows marked improvement. This enhancement in catalytic activity could originate from the additional redox activity introduced by **HL**<sub>1</sub> coordination and/or be due to the flexible nature of **HL**<sub>1</sub>.

To investigate the role of **HL**<sub>1</sub> in enhancing the catalytic activity of the metal complex, four new ternary copper(II) complexes **4**, **5**, **6**, and **7** were prepared using **HL**<sub>2</sub> [**HL**<sub>2</sub> = bis(pyridin-2-ylmethyl)amine] and **L**<sub>3</sub> [**L**<sub>3</sub> = 2,6-di(pyridin-2-yl)pyridine] in place of **HL**<sub>1</sub> (see the Experimental section). These complexes were characterized by various analytical techniques (see the Experimental section). The single crystal structures of complexes **4**, **5** and **6** were determined. The perspective ORTEP views of complexes **4**, **5** and **6** are shown in Fig. S1 and S2 (see the ESI†). The crystallographic data are given in Tables S2 and S3.† The structures of these complexes are shown in Fig. 6.

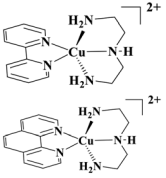
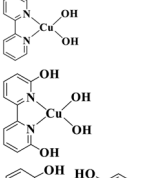
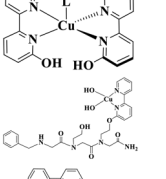
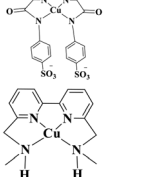
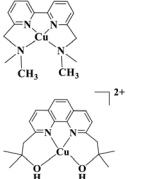

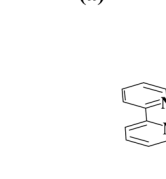
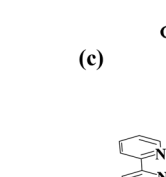
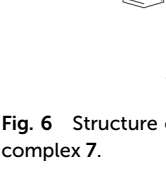

Ligands **HL**<sub>2</sub> and **L**<sub>3</sub> are both tridentate ligands but have different skeletal flexibility compared to **HL**<sub>1</sub>, with **HL**<sub>1</sub> being the most flexible and **L**<sub>3</sub> the least. The structures of ligands **HL**<sub>1</sub>, **HL**<sub>2</sub> and **L**<sub>3</sub> are shown in Fig. 7.

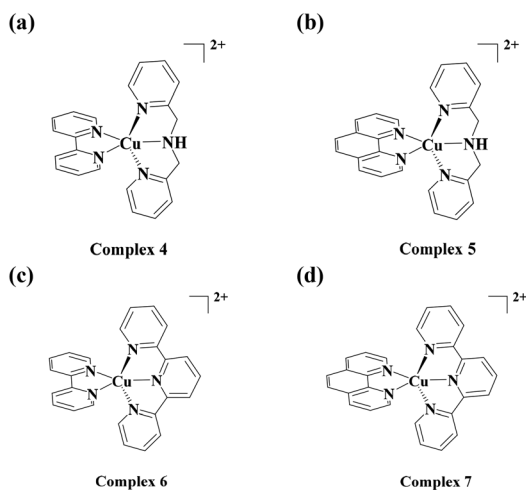
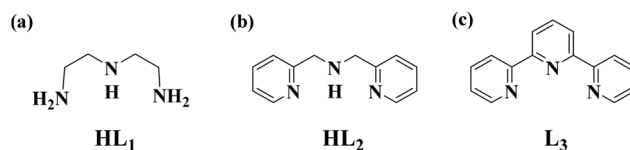
**HL**<sub>1</sub> and **HL**<sub>2</sub> are redox active, whereas, **L**<sub>3</sub> is redox inactive, as evidenced by their CVs and DPVs recorded in neutral phosphate buffer (Fig. S46†). Electrochemical investigations (Fig. S47–S53†) show that complexes **4** and **5** exhibit lower catalytic activity compared to complexes **1** and **2**, while complexes **6** and **7** show no catalytic activity. The overpotential and  $k_{\text{cat}}$  values calculated for complexes **1**, **2**, **4** and **5** are listed in Table 2.

These data clearly indicate that the flexible nature of ligand **HL**<sub>1</sub> plays an important role in the catalytic activity of the ternary metal complexes.



**Table 1** Catalytic parameter of some bipyridine and phenanthroline based copper(II) complexes

Catalyst	pH	Overpotential (mV)	$k_{\text{cat}}$ (s <sup>-1</sup> )	Ref.
	7	453	483	This work
	7	493	445	This work
	12.5	750	100	10
	12.4	640	0.4	29
	12.6	477	0.356	30
	11.5	800	5.8	23
	11.6	830	10.5	31
	9	870	0.06	32
	9	600	0.11	32
	8.4	1100	131.6	11

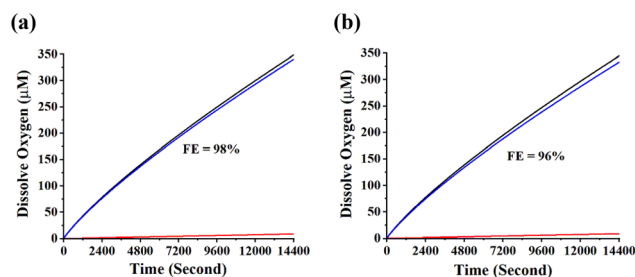
**Fig. 6** Structure of (a) complex 4, (b) complex 5, (c) complex 6 and (d) complex 7.**Fig. 7** (a) Structure of ligand HL<sub>1</sub> [N<sup>1</sup>-(2-aminoethyl)ethane-1,2-diamine], (b) structure of ligand HL<sub>2</sub> [bis(pyridin-2-ylmethyl)amine] and (c) structure of ligand L<sub>3</sub> [2,6-di(pyridin-2-yl)pyridine].**Table 2** The overpotential and  $k_{\text{cat}}$  values calculated for complexes 1, 2, 4 and 5

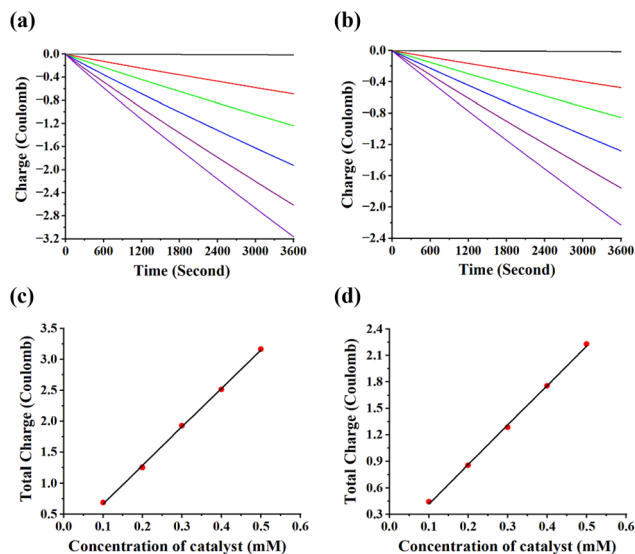
Catalyst	Overpotential (mV)	$k_{\text{cat}}$ (s <sup>-1</sup> )
1, [Cu(bipy)(HL <sub>1</sub> )](ClO <sub>4</sub> ) <sub>2</sub>	453	483
2, [Cu(phen)(HL <sub>1</sub> )](ClO <sub>4</sub> ) <sub>2</sub>	493	445
4, [Cu(bipy)(HL <sub>2</sub> )](ClO <sub>4</sub> ) <sub>2</sub>	903	39
5, [Cu(phen)(HL <sub>2</sub> )](ClO <sub>4</sub> ) <sub>2</sub>	913	34

### Controlled potential electrolysis

To measure the faradaic efficiency of the catalytic reactions, oxygen evolution was investigated through controlled potential electrolysis (CPE) at 1.32 and 1.34 V vs. NHE for complexes 1 and 2, respectively, using a large surface-area ITO working electrode (4 cm<sup>2</sup>) in a gas-tight cell (Fig. S54†). Oxygen formed in the solution was measured using a calibrated Ocean Optics FOXY probe. Faradaic efficiencies close to 98% and 96% (Fig. 8) were estimated for complexes 1 and 2, respectively, during 4 hours of bulk electrolysis experiment.

The cyclic voltammograms and UV-visible spectra of the complexes recorded before and after the bulk electrolysis experiment were almost identical (Fig. S57 and S59†). The cyclic voltammograms recorded with the ITO working electrode before and after the bulk electrolysis experiment in the absence of the catalyst were essentially identical (Fig. S61†). The FE-SEM and EDX data of fresh and used ITO working electrodes show no evidence of deposition of the electroactive species on the working electrode surface during long term electrolysis experiments for complexes 1 and 2 (Fig. S63†).

**Fig. 8** Oxygen evolution during the CPE experiment with an ITO electrode (area = 4 cm<sup>2</sup>) for (a) complex 1 and (b) complex 2 at 1.32 and 1.34 V vs. NHE respectively for 4 hours with (blue line) and without copper complexes (red line). The black line indicates the theoretical amount of oxygen as assumed by charge passed with 100% faradaic efficiency.



**Fig. 9** Plot of charge vs. time recorded during bulk electrolysis of (a) complex 1 and (b) complex 2 at 0.0 mM (black), 0.1 mM (red), 0.2 mM (green), 0.3 mM (blue), 0.4 mM (navy) and 0.5 mM (purple) concentrations at 1.32 V vs. NHE and 1.34 V vs. NHE respectively. Plot of total charge vs. concentration of (c) complex 1 and (d) complex 2 after 1 hour of electrolysis.

The total charge passed after 1 h of electrolysis under the same conditions varied linearly with the initial concentration of the complexes (Fig. 9) with no evidence of an induction period at an early stage of electrolysis, providing evidence for homogeneous single site water oxidation catalysis. The lack of evidence for a new electroactive species which is either adsorbed on the working electrode or present in the electrolyte mixture is collectively consistent with homogeneous catalysis.

## Conclusions

In conclusion, the mononuclear Cu(II) ternary complexes 1 and 2, featuring a mixed environment of pyridyl-based and aliphatic amine ligand frameworks, exhibit high electrocatalytic water oxidation activity at lower overpotentials under neutral pH conditions. These ternary complexes demonstrate superior catalytic performance compared to their binary counterparts. The ligand complementarity in ternary Cu(II) complexes enhances the stability and redox activity, both of which are crucial for high catalytic performance. Electrochemical investigations reveal that the skeletal flexibility of the aliphatic amine ligand moiety significantly influences the overall catalytic efficiency of these metal complexes.

## Experimental section

### Materials and methods

All reagents and solvents were purchased from commercial sources and were of reagent grade. UV-visible spectra were

recorded on a Cary-60 UV-visible spectrophotometer. FT-IR spectra were recorded on a Cary 630 spectrophotometer with the sample prepared as KBr pellets. The magnetic moment of the complex was measured on a Cambridge magnetic balance. Conductivity measurements were recorded using a Eutech instrument CON 700. Elemental analyses were carried out on a Thermo Scientific Flashmart Analyzer. Electrochemical measurements were made using a CHI 7035E bipotentiostat. A Carl Zeiss Supra 55 electron microscope was used for Field Emission Scanning Electron Microscopy (FE-SEM) studies after Au coating. A 20 kV electron beam was used for the collection of EDX spectra. Powder X-ray diffraction (PXRD) data were collected from 5 to 500  $2\theta$  using a Bruker-D8 Advance X-ray diffractometer. The single crystal data were collected on a Bruker Smart Apex Duo diffractometer, utilizing MoK $\alpha$  radiation ( $\lambda = 0.71073$  Å).

### Synthesis of complex 1, [Cu(bipy)(HL<sub>1</sub>)](ClO<sub>4</sub>)<sub>2</sub>

2,2'-Bipyridine (bipy) (0.50 g, 3.2 mmol) was dissolved in 10 mL of methanol and to this solution, *N*<sup>1</sup>-(2-aminoethyl) ethane-1,2-diamine (HL<sub>1</sub>) (0.33 g, 3.2 mmol) dissolved in 10 mL of methanol was added. To the resulting solution, copper(II) perchlorate hexahydrate, [Cu(H<sub>2</sub>O)<sub>6</sub>](ClO<sub>4</sub>)<sub>2</sub> (1.18 g, 3.2 mmol) dissolved in 15 mL of methanol was added dropwise, which resulted in the appearance of a dark blue precipitate. After 1 hour, the resulting mixture was filtered and the precipitate was dissolved in a methanol–water mixture and kept for crystallization at room temperature, which resulted in dark blue crystalline compounds. Yield: 1.12 g (~92%). Elemental analyses: calcd for C<sub>14</sub>H<sub>21</sub>N<sub>5</sub>Cl<sub>2</sub>O<sub>8</sub>Cu: C, 32.23; H, 4.06; N, 13.42. Found (%): C, 32.29; H, 4.02; N, 13.46. UV-visible (methanol):  $\lambda_{\text{max}}$ , 648 nm ( $\epsilon = 344$  M<sup>-1</sup> cm<sup>-1</sup>). FT-IR (KBr pellet): 3425, 3232, 3125, 2918, 1598, 1432, 1092 cm<sup>-1</sup>. Molar conductance: 209 S cm<sup>2</sup> mol<sup>-1</sup> (acetonitrile). The observed magnetic moment is found to be 1.75  $\mu_{\text{B}}$ .

### Synthesis of complex 2, [Cu(phen)(HL<sub>2</sub>)](ClO<sub>4</sub>)<sub>2</sub>

1,10-Phenanthroline (phen) (0.50 g, 2.5 mmol) was dissolved in 10 mL of methanol and to this solution *N*<sup>1</sup>-(2-aminoethyl) ethane-1,2-diamine (HL<sub>1</sub>) (0.26 g, 2.5 mmol) dissolved in 10 mL of methanol was added. To the resulting solution, copper(II) perchlorate hexahydrate, [Cu(H<sub>2</sub>O)<sub>6</sub>](ClO<sub>4</sub>)<sub>2</sub> (0.93 g, 2.5 mmol) dissolved in 15 mL of methanol was added dropwise, which resulted in the appearance of a dark blue colour precipitate. After 1 hour, the resulting mixture was filtered and the precipitate was dissolved in the methanol–water mixture and kept for crystallization at room temperature, which resulted in dark blue crystalline compounds. Yield: 1.068 g (~89%). Elemental analyses: calcd for C<sub>16</sub>H<sub>21</sub>N<sub>5</sub>Cl<sub>2</sub>O<sub>8</sub>Cu: C, 35.21; H, 3.88; N, 12.83. Found (%): C, 35.25; H, 3.84; N, 12.89. UV-visible (methanol):  $\lambda_{\text{max}}$ , 634 nm ( $\epsilon = 336$  M<sup>-1</sup> cm<sup>-1</sup>). FT-IR (KBr pellet): 3451, 3218, 3111, 2932, 1519, 1434, 1085 cm<sup>-1</sup>. Molar conductance: 206 S cm<sup>2</sup> mol<sup>-1</sup> (acetonitrile). The observed magnetic moment is found to be 1.73  $\mu_{\text{B}}$ .

### Synthesis of complex 3, [Cu(HL<sub>1</sub>)Br]Br

*N*<sup>1</sup>-(2-Aminoethyl)ethane-1,2-diamine (HL<sub>1</sub>) (0.20 g, 1.9 mmol) was dissolved in 10 mL of acetonitrile. To this solution, copper

(ii) bromide,  $\text{CuBr}_2$  (0.44 g, 1.9 mmol) dissolved in 25 ml of acetonitrile was added dropwise, which resulted in the appearance of a dark blue precipitate. After 1 hour, the resulting mixture was filtered and the precipitate was dissolved in the methanol–water mixture and kept for crystallization at room temperature, which resulted in dark blue crystalline compounds. Yield: 0.62 g (~88%). Elemental analyses: calcd for  $\text{C}_4\text{H}_{12}\text{N}_3\text{Br}_2\text{Cu}$ : C, 14.76; H, 3.72; N, 12.91. Found (%): C, 14.72; H, 4.04; N, 12.93. FT-IR (KBr): 3431, 3234, 3139, 2922, 1585, 1082  $\text{cm}^{-1}$ . Molar conductance: 118  $\text{S cm}^2 \text{mol}^{-1}$  (acetonitrile). The observed magnetic moment is found to be  $1.65\mu_{\text{B}}$ .

#### Synthesis of complex 4, $[\text{Cu}(\text{bipy})(\text{HL}_2)](\text{ClO}_4)_2$

2,2'-Bipyridine (bipy) (0.50 g, 3.2 mmol) was dissolved in 10 mL of methanol and to this solution bis(pyridin-2-ylmethyl)amine ( $\text{HL}_2$ ) (0.64 g, 3.2 mmol) dissolved in 10 mL of methanol was added. To the resulting solution, copper(II) perchlorate hexahydrate,  $[\text{Cu}(\text{H}_2\text{O})_6](\text{ClO}_4)_2$  (1.18 g, 3.2 mmol) dissolved in 15 mL of methanol was added dropwise, which resulted in the appearance of a blue precipitate. After 1 hour, the resulting mixture was filtered and the precipitate was dissolved in the methanol–water mixture and kept for crystallization at room temperature, which resulted in blue crystalline compounds. Yield: 1.21 g (~94%). Elemental analyses: calcd for  $\text{C}_{22}\text{H}_{21}\text{N}_5\text{Cl}_2\text{O}_8\text{Cu}$ : C, 42.77; H, 3.43; N, 11.33. Found (%): C, 42.74; H, 3.42; N, 11.36. FT-IR (KBr): 3465, 3051, 2868, 1605, 1442, 1143, 1116, 1082  $\text{cm}^{-1}$ . Molar conductance: 211  $\text{S cm}^2 \text{mol}^{-1}$  (acetonitrile). The observed magnetic moment is found to be  $1.72\mu_{\text{B}}$ .

#### Synthesis of complex 5, $[\text{Cu}(\text{phen})(\text{HL}_2)](\text{ClO}_4)_2$

1,10-Phenanthroline (phen) (0.50 g, 2.5 mmol) was dissolved in 10 mL of methanol and to this solution bis(pyridin-2-ylmethyl)amine ( $\text{HL}_2$ ) (0.50 g, 2.5 mmol) dissolved in 10 mL of methanol was added. To the resulting solution, copper(II) perchlorate hexahydrate,  $[\text{Cu}(\text{H}_2\text{O})_6](\text{ClO}_4)_2$  (0.93 g, 2.5 mmol) dissolved in 15 mL of methanol was added dropwise, which resulted in the appearance of a blue precipitate. After 1 hour, the resulting mixture was filtered and the precipitate was dissolved in the methanol–water mixture and kept for crystallization at room temperature which resulted in blue crystalline compounds. Yield: 1.19 g (~88%). Elemental analyses: calcd for  $\text{C}_{24}\text{H}_{21}\text{N}_5\text{Cl}_2\text{O}_8\text{Cu}$ : C, 44.91; H, 3.30; N, 10.91. Found (%): C, 44.92; H, 3.28; N, 10.88. FT-IR (KBr): 3438, 3024, 2882, 1598, 1428, 1136, 1109, 1096  $\text{cm}^{-1}$ . Molar conductance: 208  $\text{S cm}^2 \text{mol}^{-1}$  (acetonitrile). The observed magnetic moment is found to be  $1.70\mu_{\text{B}}$ .

#### Synthesis of complex 6, $[\text{Cu}(\text{bipy})(\text{L}_3)](\text{ClO}_4)_2$

2,2'-Bipyridine (bipy) (0.50 g, 3.2 mmol) was dissolved in 10 mL of methanol and to this solution 2,6-di(pyridin-2-yl)pyridine ( $\text{L}_3$ ) (0.75 g, 3.2 mmol) dissolved in 10 mL of methanol was added. To the resulting solution, copper(II) perchlorate hexahydrate,  $[\text{Cu}(\text{H}_2\text{O})_6](\text{ClO}_4)_2$  (1.18 g, 3.2 mmol) dissolved in 15 mL of methanol was added dropwise, which resulted in the appearance of a light green precipitate. After 1 hour, the resulting mixture was filtered and the precipitate was dissolved in the methanol–water mixture

and kept for crystallization at room temperature which resulted in light green crystalline compounds. Yield: 1.25 g (~90%). Elemental analyses: calcd for  $\text{C}_{25}\text{H}_{19}\text{N}_5\text{Cl}_2\text{O}_8\text{Cu}$ : C, 46.06; H, 2.94; N, 10.74. Found (%): C, 46.08; H, 2.92; N, 10.75. FT-IR (KBr): 3621, 3397, 3044, 1591, 1448, 1136, 1116, 1082  $\text{cm}^{-1}$ . Molar conductance: 210  $\text{S cm}^2 \text{mol}^{-1}$  (acetonitrile). The observed magnetic moment is found to be  $1.76\mu_{\text{B}}$ .

#### Synthesis of complex 7, $[\text{Cu}(\text{phen})(\text{L}_3)](\text{ClO}_4)_2$

1,10-Phenanthroline (phen) (0.50 g, 2.5 mmol) was dissolved in 10 mL of methanol and to this solution 2,6-di(pyridin-2-yl)pyridine ( $\text{L}_3$ ) (0.59 g, 2.5 mmol) dissolved in 10 mL of methanol was added. To the resulting solution, copper(II) perchlorate hexahydrate,  $[\text{Cu}(\text{H}_2\text{O})_6](\text{ClO}_4)_2$  (0.93 g, 2.5 mmol) dissolved in 15 mL of methanol was added dropwise, which resulted in the appearance of a light green precipitate. After 1 hour, the resulting mixture was filtered and the precipitate was dissolved in the methanol–water mixture and kept for crystallization at room temperature which resulted in light green crystalline compounds. Yield: 1.27 g (~91%). Elemental analyses: calcd for  $\text{C}_{27}\text{H}_{19}\text{N}_5\text{Cl}_2\text{O}_8\text{Cu}$ : C, 47.98; H, 2.83; N, 10.36. Found (%): C, 47.95; H, 2.84; N, 10.38. FT-IR (KBr): 3486, 3418, 3064, 1605, 1442, 1136, 1116, 1082  $\text{cm}^{-1}$ . Molar conductance: 205  $\text{S cm}^2 \text{mol}^{-1}$  (acetonitrile). The observed magnetic moment is found to be  $1.74\mu_{\text{B}}$ .

## Data availability

The data supporting this article have been included as part of the ESI.† Crystallographic data for the structures reported in this article have been deposited with the Cambridge Crystallographic Data Centre (CCDC) under deposition numbers 2401171, 2401172, 2435313–2435318.†

## Conflicts of interest

There are no conflicts to declare.

## Acknowledgements

A. K. would like to thank the Department of Science and Technology (SERB), India, for financial support (award no. YSS/2015/000878). The authors are also grateful to the Department of Chemistry, IISER Pune for single crystal XRD data and SIC, IIT Indore for FESEM and EDX data. P. D. gratefully acknowledges UGC for providing research fellowships (Student ID: 2047/(CSIR-UGC NET JUNE 2019)).

## References

- 1 P. Hota, A. Das and D. K. Maiti, A short review on generation of green fuel hydrogen through water splitting, *Int. J. Hydrogen Energy*, 2023, **48**, 523–541.

- 2 L. Quan, H. Jiang, G. Mei, Y. Sun and B. You, Bifunctional electrocatalysts for overall and hybrid water splitting, *Chem. Rev.*, 2024, **124**, 3694–3812.
- 3 J. H. Kim, D. Hansora, P. Sharma, J.-W. Jang and J. S. Lee, Toward practical solar hydrogen production – an artificial photosynthetic leaf-to-farm challenge, *Chem. Soc. Rev.*, 2019, **48**, 1908–1971.
- 4 J. Yano and V. Yachandra,  $\text{Mn}_4\text{Ca}$  cluster in photosynthesis: Where and how water is oxidized to dioxygen, *Chem. Rev.*, 2014, **114**, 4175–4205.
- 5 G. Chen, Z.-W. Chen, Y.-M. Wang, P. He, C. Liu, H.-X. Tong and X.-Y. Yi, Efficient electrochemical water oxidation mediated by pyridylpyrrole–carboxylate ruthenium complexes, *Inorg. Chem.*, 2021, **60**, 15627–15634.
- 6 G. Maayan, N. Gluz and G. Christou, A bioinspired soluble manganese cluster as a water oxidation electrocatalyst with low overpotential, *Nat. Catal.*, 2017, **1**, 48–54.
- 7 V. K. K. Praneeth, M. Kondo, M. Okamura, T. Akai, H. Izu and S. Masaoka, Pentanuclear iron catalysts for water oxidation: Substituents provide two routes to control onset potentials, *Chem. Sci.*, 2019, **10**, 4628–4639.
- 8 M. Bera, S. Kaur, K. Keshari, D. Moonshiram and S. Paria, Characterization of reaction intermediates involved in the water oxidation reaction of a molecular cobalt complex, *Inorg. Chem.*, 2022, **61**, 21035–21046.
- 9 M. Zhang, M.-T. Zhang, C. Hou, Z. F. Ke and T. B. Lu, Homogeneous electrocatalytic water oxidation at neutral pH by a robust macrocyclic nickel(II) complex, *Angew. Chem., Int. Ed.*, 2014, **53**, 13042–13048.
- 10 S. M. Barnett, K. I. Goldberg and J. M. Mayer, A soluble copper–bipyridine water-oxidation electrocatalyst, *Nat. Chem.*, 2012, **4**, 498–502.
- 11 Q.-F. Chen, Z.-Y. Cheng, R.-Z. Liao and M.-T. Zhang, Bioinspired trinuclear copper catalyst for water oxidation with a turnover frequency up to  $20000\text{ s}^{-1}$ , *J. Am. Chem. Soc.*, 2021, **143**, 19761–19768.
- 12 S. Khan, S. Sengupta, M. A. Khan, M. P. Sk, N. C. Jana and S. Naskar, Electrocatalytic water oxidation by mononuclear copper complexes of bis-amide ligands with  $\text{N}_4$  donor: Experimental and theoretical investigation, *Inorg. Chem.*, 2024, **63**, 1888–1897.
- 13 P. Garrido-Barros, I. Funes-Ardoiz, S. Drouet, J. Benet-Buchholz, F. Maseras and A. Llobet, Redox non-innocent ligand controls water oxidation overpotential in a new family of mononuclear Cu-based efficient catalysts, *J. Am. Chem. Soc.*, 2015, **137**, 6758–6761.
- 14 J. Shen, M. Wang, J. Gao, H. Han, H. Liu and L. Sun, Improvement of electrochemical water oxidation by fine-tuning the structure of tetradentate  $\text{N}_4$  ligands of molecular copper catalysts, *ChemSusChem*, 2017, **10**, 4581–4588.
- 15 H. Kuilya, N. Alam, D. Sarma, D. Choudhury and A. Kalita, Ligand assisted electrocatalytic water oxidation by a copper (II) complex in neutral phosphate buffer, *Chem. Commun.*, 2019, **55**, 5483–5486.
- 16 S. Chattopadhyay, A. Ghatak, Y. Ro, R. Guillot, Z. Halime, A. Aukauloo and A. Dey, Ligand radical mediated water oxidation by a family of copper o-phenylene bis-oxamate complexes, *Inorg. Chem.*, 2021, **60**, 9442–9455.
- 17 J. Lin, N. Wang, X. Chen, X. Yang, L. Hong, Z. Ruan, H. Ye, Y. Chen and X. Liang, Electrocatalytic water oxidation by copper(II) complexes with a pentadentate amine-pyridine ligand, *Sustainable Energy Fuels*, 2022, **6**, 1312–1318.
- 18 K. Yu, T. Wang, Y. Sun, M. Kang, X. Wang, D. Zhu, S. Xue, J. Shen, Q. Zhang and J. Liu, Impact of the hybridization form of the coordinated nitrogen atom on the electrocatalytic water oxidation performance of copper complexes with pentadentate amine-pyridine ligands, *Dalton Trans.*, 2024, **53**, 612–618.
- 19 H. Kuilya, P. Das, S. Basak, D. Sarma, P. Mazumdar, D. Choudhury and A. Kalita, Effect of ligand substituents on the reactivity pathways of copper(II) complexes towards electrocatalytic water oxidation, *Dalton Trans.*, 2024, **53**, 17547–17553.
- 20 X.-J. Su, C. Zheng, Q.-Q. Hu, H.-Y. Du, R.-Z. Liao and M.-T. Zhang, Bimetallic cooperative effect on O–O bond formation: Copper polypyridyl complexes as water oxidation catalyst, *Dalton Trans.*, 2018, **47**, 8670–8675.
- 21 X. Zhang, Y.-Y. Li, J. Jiang, R. Zhang, R.-Z. Liao and M. Wang, A dinuclear copper complex featuring a flexible linker as water oxidation catalyst with an activity far superior to its mononuclear counterpart, *Inorg. Chem.*, 2020, **59**, 5424–5432.
- 22 K. J. Fisher, K. L. Materna, B. Q. Mercado, R. H. Crabtree and G. W. Brudvig, Electrocatalytic water oxidation by a copper(II) complex of an oxidation-resistant ligand, *ACS Catal.*, 2017, **7**, 3384–3387.
- 23 T. Ghosh, P. Ghosh and G. Maayan, A copper-peptoid as a highly stable, efficient, and reusable homogeneous water oxidation electrocatalyst, *ACS Catal.*, 2018, **8**, 10631–10640.
- 24 P. Garrido-Barros, D. Moonshiram, M. Gil-Sepulcre, P. Pelosin, C. Gimbert-Suriñach, J. Benet-Buchholz and A. Llobet, Redox metal–ligand cooperativity enables robust and efficient water oxidation catalysis at neutral pH with macrocyclic copper complexes, *J. Am. Chem. Soc.*, 2020, **142**, 17434–17446.
- 25 J. Shen, X. Zhang, M. Cheng, J. Jiang and M. Wang, Electrochemical water oxidation catalyzed by  $\text{N}_4$ -coordinate copper complexes with different backbones: Insight into the structure–activity relationship of copper catalysts, *ChemCatChem*, 2020, **12**, 1302–1306.
- 26 Q.-F. Chen, K.-L. Xian, H.-T. Zhang, X.-J. Su, R.-Z. Liao and M.-T. Zhang, Pivotal role of geometry regulation on O–O bond formation mechanism of bimetallic water oxidation catalysts, *Angew. Chem., Int. Ed.*, 2024, **63**, e202317514.
- 27 M.-T. Zhang, Z. Chen, P. Kang and T. J. Meyer, Electrocatalytic water oxidation with a copper(II) polypeptide complex, *J. Am. Chem. Soc.*, 2013, **135**, 2048–2051.
- 28 K. Yu, Y. Sun, D. Zhu, Z. Xu, J. Wang, J. Shen, Q. Zhang and W. Zhao, A low-cost commercial Cu(II)–EDTA complex for electrocatalytic water oxidation in neutral aqueous solution, *Chem. Commun.*, 2022, **58**, 12835–12838.



- 29 T. Zhang, C. Wang, S. Liu, J.-L. Wang and W. Lin, A biomimetic copper water oxidation catalyst with low overpotential, *J. Am. Chem. Soc.*, 2014, **136**, 273–281.
- 30 D. L. Gerlach, S. Bhagan, A. A. Cruce, D. B. Burks, I. Nieto, H. T. Truong, S. P. Kelley, C. J. Herbst-Gervasoni, K. L. Jernigan, M. K. Bowman, S. Pan, M. Zeller and E. T. Papish, Studies of the pathways open to copper water oxidation catalysts containing proximal hydroxy groups during basic electrocatalysis, *Inorg. Chem.*, 2014, **53**, 12689–12698.
- 31 M. Gil-Sepulcre, P. Garrido-Barros, J. Oldengott, I. Funes-Ardoiz, R. Bofill, X. Sala, J. Benet-Buchholz and A. Llobet, Consecutive ligand-based electron transfer in new molecular copper-based water oxidation catalysts, *Angew. Chem., Int. Ed.*, 2021, **60**, 18639–18644.
- 32 J. Wang, Y. Ping, Y. Chen, S. Liu, J. Dong, Z. Ruan, X. Liang and J. Lin, Improvement of electrocatalytic water oxidation activity of novel copper complex by modulating the axial coordination of phosphate on metal center, *Dalton Trans.*, 2024, **53**, 5222–5229.
- 33 S. Basak, P. Das, H. Kuilya, D. Choudhury and A. Kalita, Electrocatalytic water oxidation activity of phenolate bridged dinuclear copper(II) complexes in alkaline phosphate buffer, *New J. Chem.*, 2025, **49**, 7134–7139.
- 34 E. Laviron, General Expression of the linear potential sweep voltammogram in the case of diffusionless electrochemical systems, *J. Electroanal. Chem.*, 1979, **101**, 19–28.
- 35 A. J. Bard and L. R. Faulkner, in *Electrochemical methods: Fundamentals and applications*, Wiley, New York, 2nd edn, 2001.
- 36 D. Wang and J. T. Groves, Efficient water oxidation catalyzed by homogeneous cationic cobalt porphyrins with critical roles for the buffer base, *Proc. Natl. Acad. Sci. U. S. A.*, 2013, **110**, 15579–15584.
- 37 Z. Chen, J. J. Concepcion, X. Hu, W. Yang, P. G. Hoertz and T. J. Meyer, Concerted O atom–proton transfer in the O–O bond forming step in water oxidation, *Proc. Natl. Acad. Sci. U. S. A.*, 2010, **107**, 7225–7229.